LETTERS
PUBLISHED ONLINE: 22 APRIL 2012 | DOI: 10.1038/NPHOTON.2012.83
nature photonics

Structured illumination microscopy using unknown speckle patterns

E. Mudry[1], K. Belkebir[1], J. Girard[1], J. Savatier[1], E. Le Moal[1], C. Nicoletti[2], M. Allain[1] and A. Sentenac[1]*

Using spatially non-uniform illumination significantly improves the resolution of light microscopy[1]. Indeed, frequency mixing between the object and the illumination permits the recovery of object frequencies beyond the diffraction-limited detection band pass[2–5]. However, the image reconstruction process requires a precise knowledge of the illumination patterns (usually focused or periodic) and therefore sophisticated stable mountings[6,7]. Here, we show, both theoretically and experimentally, that image reconstruction can be performed without knowing the illumination patterns, provided that their average is roughly homogeneous over the sample. Using blind structured illumination microscopy (blind-SIM), a resolution about two times better than that of conventional wide-field microscopy is obtained by simply illuminating the sample with several uncontrolled random speckles. Our approach is insensitive to specimen or aberration-induced illumination deformations, does not require any calibration step or stringent control of the illumination, and dramatically simplifies the experimental set-up.

In classical wide-field fluorescence microscopy, the sample fluorescence is excited by a uniform light intensity and the emitted fluorescence is detected at the image plane of a microscope objective. In the linear regime, the recorded intensity M can be modelled as the convolution of the fluorescence density of the sample ρ with the microscope detection point spread function h. The image resolution is limited by the spectral band pass of h, the cutoff of which is fixed by $\nu_{\max} = 2\mathrm{NA}/\lambda_{\mathrm{em}}$, where λ_{em} is the emitted wavelength and NA is the numerical aperture of the microscope objective. To improve the frequency content of the image, a widespread solution consists of illuminating the sample with a non-uniform light pattern. In this case, the recorded intensity is given by

$$M = (I\rho) * h \qquad (1)$$

where $*$ indicates the convolution product and I is the spatially varying illumination intensity. If the illumination largest spatial frequency allowed by the excitation band pass is ν_i, the convolution theorem shows that M depends on the spatial frequencies of ρ up to $\nu_{\max} + \nu_i$. Thus, the recorded intensity map contains sample information that is beyond the detection band pass. Many imaging approaches exhibiting a resolution that is better than that of classical wide-field microscopy (including structured illumination fluorescence microscopy (SIM) with periodic excitation patterns[2,3,8] or near-field hot spots[9,10], tomographic diffraction microscopy with rotating plane waves or translating speckles[4,11–14] and even confocal or related microscopies with focused excitation spots[15,16]) rest on this principle.

However, although these approaches demonstrate resolutions up to two times better than that of the wide-field microscope[1,7], they are still rarely used in the microscopy community, largely because they all rely on reconstruction algorithms that require a precise knowledge of the illumination patterns, with small errors in the latter yielding artefacts in the final high-resolution image. This important constraint can be overcome only if the illumination distortion induced by the sample or the objective aberrations is negligible and if the set-ups are carefully calibrated and stabilized to control the illumination. This limits the application domain to weakly scattering samples and makes the experimental implementation very technical. Hence, a major step forward to extend the potential of SIM techniques is to develop a method, hereafter named blind-SIM, that is able to retrieve the sample fluorescence density without *a priori* information on the illumination patterns.

To address the blind-SIM issue, we consider an experimental configuration in which a fluorescent sample is successively illuminated by L different light patterns $I_{l=1,\ldots,L}$. The fluorescence density ρ is linked to the L images $M_{l=1,\ldots,L}$ by

$$M = (I_l\rho) * h \qquad (2)$$

Given the L images, we seek to reconstruct both the fluorescence density and the L incident intensities, that is, $L+1$ unknowns. The system is thus highly underdetermined. To avoid this problem, we introduce the constraint that the sum of all the incident

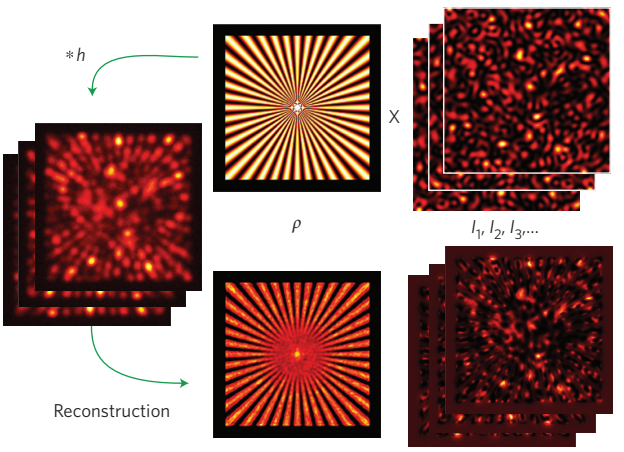

Figure 1 | Illustration of the different steps of a simulated speckle blind-SIM experiment. A total of 160 different speckle patterns with $\mathrm{NA}_{\mathrm{eff}} = \mathrm{NA}$ (upper right panel) are multiplied by the sample fluorophore density pattern (upper centre) and convolved by the microscope detection point spread function. The data are corrupted by Poisson and electronic noise to yield 160 low-resolution images (left panel). The reconstruction algorithm simultaneously estimates the image of the fluorescence density (lower centre panel) and the 160 speckle patterns (lower right panel). All details of the simulation parameters are provided in the Supplementary Section II A.

[1]Institut Fresnel (CNRS UMR 7249), Université Aix-Marseille, Campus de St Jérôme, 13013 Marseille, France, [2]ISM2 (CNRS UMR 7313) Université Aix-Marseille, Campus de St Jérôme, 13013 Marseille, France. *e-mail: anne.sentenac@fresnel.fr

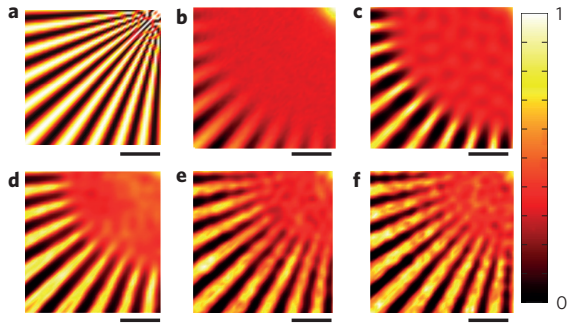

Figure 2 | Numerical study of the resolution of the reconstructed sample using speckle blind-SIM versus the excitation pattern spectrum. **a**, Fluorescence density of the object. **b**, Image of the object obtained with uniform illumination and an oil objective microscope (NA = 1.49). **c**, Deconvolution of the wide-field image shown in **b**. **d**, Fluorescence density reconstructed by blind-SIM from $L = 160$ images obtained with speckle illuminations. The random speckles are generated with an effective numerical aperture that is half that of the detection, $NA_{eff} = 0.5NA$. **e**, As in **d**, but $NA_{eff} = NA$. **f**, As in **d**, but $NA_{eff} = 1.5NA$. The black bar corresponds to the incident and emitted wavelength λ. The colour scale represents the normalized fluorophore density. For a fair comparison, the experiments have the same photon budget and the deconvolution procedure includes the same regularization terms as blind-SIM. Details of the simulation and regularization procedure are provided in the Supplementary Section II A.

intensities be roughly homogeneous over the sample plane. This condition assumes that the sample is uniformly illuminated, on average. It reads,

$$\sum_{l=1}^{L} I_l \approx LI_0$$

where I_0 is constant over the sample plane. We use this constraint to reduce the number of unknowns. The last intensity I_L is assumed to be equal to

$$I_L = LI_0 - \sum_{l=1}^{L-1} I_l$$

so that the Lth equation (2) can be expressed as

$$M_L = \left[\left(LI_0 - \sum_{l=1}^{L-1} I_l\right)\rho\right] * h$$

where I_L is now absent. The fluorescence density and the $L-1$ first illuminations are then jointly estimated in an iterative way so as to minimize the cost functional,

$$F(\rho, I_{l=1,\ldots,L-1}) = \sum_{l=1}^{L-1} \|M_l - (I_l\rho) * h\|^2 + \left\|M_L - \left[\left(LI_0 - \sum_{l=1}^{L-1} I_l\right)\rho\right] * h\right\|^2$$

where $\|.\|$ is an euclidian norm over the image space. A conjugate gradient algorithm is then used to modify the estimates of ρ and $I_{l=1,\ldots,L-1}$ in such a way that F decreases. To regularize further the inversion problem, ρ, $I_{l=1,\ldots,L-1}$ are assumed to be positive. Note that with this approach, the residual inhomogeneity of the illumination average will be transferred to the reconstructed fluorescence density. A detailed description of the blind-SIM algorithm can be found in Supplementary Section I.

In the following, the improvement in resolution provided by our method is demonstrated by comparing blind-SIM images to classical wide-field images obtained under uniform illumination. For a fair comparison, all the wide-field images were deconvolved with a nonlinear iterative technique that included the same regularization terms (in particular the positivity constraint) as the blind-SIM algorithm, and we were careful that the experiments had the same photon budget.

We first investigated the performances of blind-SIM on simulated images of a flat two-dimensional fluorescent sample placed at the focal plane of a microscope objective with numerical aperture NA = 1.49. The sample was illuminated by 160 different fully developed speckles as illustrated in Fig. 1. The speckles were calculated as a sum of plane waves for which the wave vector transverse projections were taken on a disk of radius $2\pi NA_{eff}/\lambda_{exc}$, where λ_{exc} is the excitation wavelength (which is equal to the emission wavelength). The images were obtained using equation (1) and corrupted with Poisson and electronic noise. In Fig. 1 we observe that the blind-SIM estimations of the fluorescence density and $L-1$ speckles are in good agreement with the actual values.

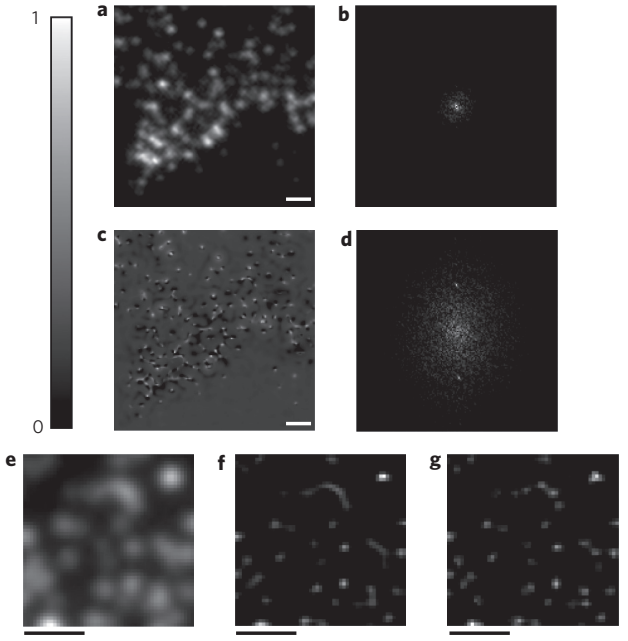

Figure 3 | Experimental periodical SIM data processed by blind-SIM. Fluorescent beads with diameters of 90 nm are illuminated by 24 different standing waves with period $d \approx 230$ nm through an oil objective (NA = 1.45) at $\lambda_{exc} = 633$ nm. **a**, One of the 24 recorded images. **b**, Absolute value of the Fourier transform of **a** (after subtracting the mean). The peaks of the light grid are not visible. **c**, Blind-SIM reconstructed excitation pattern of the image in **a**. The pattern is reconstructed only where the reconstructed fluorescence density is non-zero. **d**, Absolute value of the Fourier transform of **c** (after subtracting the mean). The peaks of the light grid are clearly visible among noise-like features, which indicate the support of the pattern reconstruction. **e**, Zoom of the sample image obtained under wide-field illumination. **f**, Deconvolution of **e**, in which closely located beads are unresolved. **g**, Blind-SIM reconstructed fluorescent density obtained from the 24 structured illumination measurements. Closely located beads are now well resolved. All scale bars, 1 μm. The grey scale represents the normalized fluorescent density. About 10,000 photons per bead are detected during the measurement process. Details of the experimental set-up and sample are provided in the Methods.

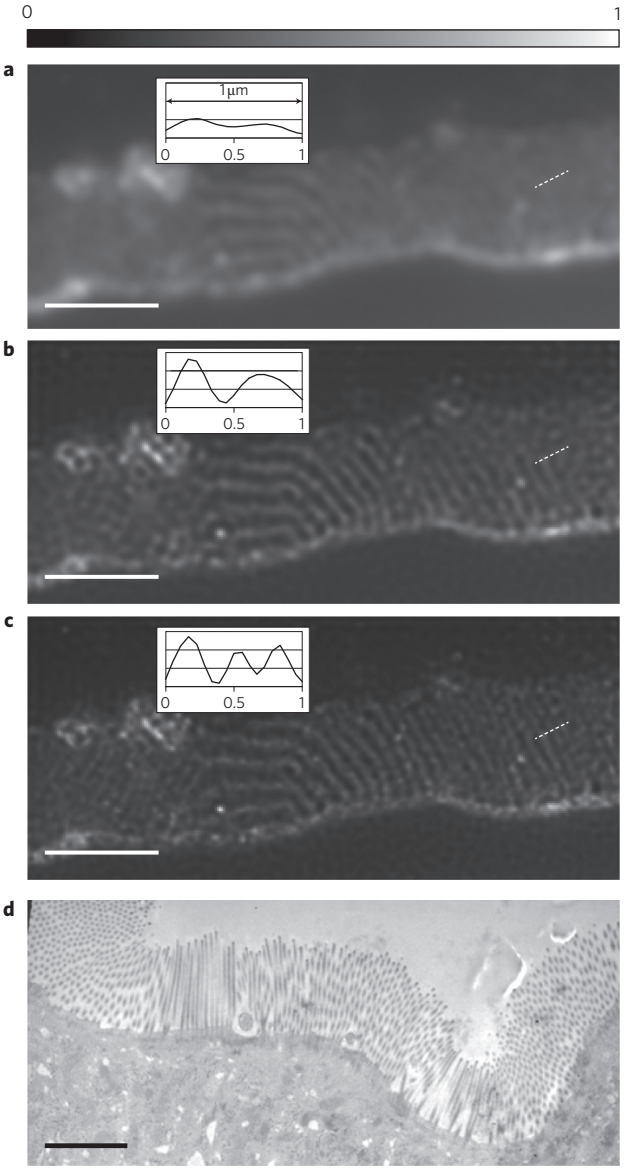

Figure 4 | Experimental speckle data processed by blind-SIM. The sample is an ultrathin (80 nm) Epon-embedded section of rabbit jejunum with glycoproteins marked with Cy5 fluorescent dye. It is illuminated by 150 uncontrolled different speckles through an oil objective (NA = 1.45) at $\lambda_{exc} = 633$ nm. **a**, Wide-field image of the sample. **b**, Deconvolution of the wide-field image in **a**. **c**, Blind-SIM fluorescence density obtained from the 150 speckle images. **d**, Image of a similar sample, using a transmission electronic microscope. Insets are plots of the image intensity along the 1 μm dashed lines. Scale bar, 3 μm. The grey scale is the normalized fluorophore density. The total number of photons per pixel, averaged over the marked microvilli region, is ~20,000. Note that the wavy lines observed in the centre of **a**–**c** are not an artefact. Similar lines made of dark points are visible on the TEM image in **d**. These arise because the microtome cuts the microvilli at an angle. Details on the experimental set-up and sample are provided in the Methods.

To verify that frequency mixing between illumination and object is at the root of the blind-SIM improvement in resolution, we considered a numerical experiment in which the same sample is illuminated by speckles with different spectra. In Fig. 2d–f, the reconstructed fluorescence densities obtained from $L = 160$ speckle images are displayed for $NA_{eff} = 0.5$ NA, $NA_{eff} = NA$ and $NA_{eff} = 1.5$ NA, respectively and compared to the true fluorescence density of the sample, the wide-field image of the sample and the deconvolution of the wide-field image (Fig. 2a–c, respectively). As expected, the resolution of the blind-SIM images is always better than that of the deconvolved image and clearly improves with increasing NA_{eff}.

This numerical analysis was completed by a quantitative study of blind-SIM resolution with respect to noise. Supplementary Section II shows that blind-SIM is always better than deconvolution. If the average photon noise is below 1% (which is the case for most wide-field images), the resolution of blind-SIM is comparable to that of classical periodic SIM (with known excitation patterns) and about half that of classical wide-field microscopy.

Blind-SIM was then validated on experimental images from a wide-field microscope with periodic excitation patterns. In total, 24 images of a sample made of 90 nm fluorescent beads were recorded for various positions and orientation of a periodic light grid (details regarding the experimental set-up and sample are given in the Methods) and processed by our algorithm. We observe that, although the excitation peaks are not visible on the Fourier transform of the raw images (Fig. 3a,b), blind-SIM accurately retrieves the light patterns (Fig. 3c,d). In this experiment, where the measured width of the detection point spread function is ~360 nm, the resolution of the blind-SIM image (Fig. 3g) is as good as that provided by an up-to-date SIM algorithm assuming the periodicity of the light pattern and reaches 160 nm. It is much better than that of the deconvolved wide-field image (Fig. 3f), which is ~250 nm. Moreover, we show in Supplementary Fig. S3 that blind-SIM is able to handle strongly distorted periodic patterns, which are beyond the reach of classical SIM algorithms.

Finally, blind-SIM was applied to the experimental microscope images of a biological sample illuminated by 150 different speckles. The speckles were obtained by moving a diffuser through the laser path in front of the microscope objective. The sample was an ultrathin (80 nm) slice of rabbit jejunum with glycoproteins marked with Cy5 fluorescent dye. The wide-field image of the sample, the deconvolution of the wide-field image and the blind-SIM density of fluorescence are shown in Fig. 4a–c, respectively. We observe a significant improvement of the resolution with blind-SIM (see also the insets of Fig. 4). Note that taking the standard variation of the speckle images (as in the dynamic speckle illumination approach[17]), while useful for removing out-of-focus fluorescence, did not yield any improvement in resolution.

In conclusion, we have developed a method (blind-SIM) that circumvents the major issue of the control and *a priori* knowledge of the excitation patterns in microscopy using non-uniform illumination. Using blind-SIM, images with a resolution about two times better than that of wide-field microscopy can be obtained by simply illuminating samples with random light speckles. Promising applications of blind-SIM include its adaptation to non-fluorescence microscopy, typically in the framework of optical diffraction tomography[4], and its extension to subdiffraction imaging, with the use of high-frequency near-field speckles or non-linear photoresponse[18–20].

Methods

Details on the simulated data used for Figs 1 and 2 can be found in Supplementary Section II.

Experimental set-up and sample used for Fig. 3. Figure 3 was obtained using a home-built SIM in epi-illumination mode. Using a glass transmission grating (holographic, 80 lines/mm) placed in a secondary image plane of the microscope and illuminated with a collimated laser beam (He–Ne, 633 nm), a sinusoidal light pattern (period, ~230 nm) was formed on the sample through a high-numerical-aperture objective (NA = 1.45, ×100, CFI Plan Apochromat, Nikon). The orientation and position of the light pattern were modified by translating and rotating the transmission grating. Only ±1 grating diffracted orders were used, the others being blocked by a diaphragm and central stop. The fluorescence light was separated from the laser reflection by a dichroic mirror and filter, and finally imaged

by an electron-multiplying charge-coupled device camera (Andor iXon 897) with a pixel size of ~100 nm (after magnification). The grating was translated eight times for three different orientations (0, 60 and 120°), yielding a total of 24 recorded images. The translation step, corresponding to a quarter of the pattern period, was calibrated by analysis of the laser reflection on the coverslip surface. To ensure the same photon budget, the wide-field image was obtained by summing the 24 structured illumination measurements. The two-dimensional detection point spread function was estimated by averaging the images of isolated fluorophores. The sample consisted of 90-nm-diameter fluorescent beads (Spherotech, SPHERO, Sky Blue) spread on a coverslip and then immersed in glycerol.

Experimental set-up and sample used for Fig. 4. The set-up used for Fig. 4 was the same as that described in the previous section except that the transmission grating was replaced by a diffuser (a grained sheet protector). Its position did not matter, as long as the back focal plane of the objective was filled with scattered light and as the diffuser was not directly imaged on the sample. In total, 150 different speckle illuminations were obtained by translating the diffuser between each image recording. To ensure the same photon budget, the wide-field image was obtained by summing the 150 speckle images.

The sample consisted of ultrathin (80 nm) Epon-embedded sections of rabbit jejunum deposited on a coverslip, the glycoproteins of which were marked with Cy5 fluorescent dye. More precisely, the tissue was fixed by immersion in 2.5% glutaraldehyde in phosphate buffer at pH 7.4 (PBS) for 1 h, followed by 2% osmium tetroxide in PBS for 1 h. The specimens were dehydrated by passage through a graded series of ethanol (70, 90 and 100%) and embedded in Epon 812. Ultrathin sections (80 nm) were obtained with a microtome and labelled with Cl 3.3 monoclonal antibody (1/100) and Cy5-conjugated goat anti mouse antibodies (1/200, Bethyl Laboratories).

Received 20 October 2011; accepted 16 March 2012; published online 22 April 2012

References

1. Heintzmann, R. & Gustafsson, M. G. L. Subdiffraction resolution in continuous samples. *Nature Photon.* **3,** 362–364 (2009).
2. Gustafsson, M. Surpassing the lateral resolution limit by a factor of two using structured illumination microscopy. *J. Microsc.* **198,** 82–87 (2000).
3. Heintzmann, R. & Cremer, C. Laterally modulated excitation microscopy: improvement of resolution by using a diffraction grating. *Proc. SPIE, Optical Biopsies and Microscopic Techniques III* **3568,** 185–196 (1999).
4. Lauer, V. New approach to optical diffraction tomography yielding a vector equation of diffraction tomography and a novel tomographic microscope. *J. Microsc.* **205,** 165–176 (2002).
5. Choi, W. *et al.* Tomographic phase microscopy. *Nature Meth.* **4,** 717–719 (2007).
6. Wilson, T. *Confocal Microscopy* (Academic Press, 1990).
7. Kner, P., Chhun, B. B., Griffis, E. R., Winoto, L. & Gustafsson, M. G. L. Super-resolution video microscopy of live cells by structured illumination. *Nature Meth.* **6,** 339–342 (2009).
8. Lukosz, W. Optical systems with resolving powers exceeding the classical limit. *J. Opt. Soc. Am.* **56,** 1463–1471 (1966).
9. Gur, A., Fixler, D., Micó, V., Garcia, J. & Zalevsky, Z. Linear optics based nanoscopy. *Opt. Express* **18,** 22222–22231 (2010).
10. Sentenac, A., Belkebir, K., Giovannini, H. & Chaumet, P. C. Subdiffraction resolution in total internal reflection fluorescence microscopy with a grating substrate. *Opt. Lett.* **33,** 255–257 (2008).
11. Maire, G. *et al.* Experimental demonstration of quantitative imaging beyond Abbé's limit with optical diffraction tomography. *Phys. Rev. Lett.* **102,** 213905 (2009).
12. García, J., Zalevsky, Z. & Fixler, D. Synthetic aperture superresolution by speckle pattern projection. *Opt. Express* **13,** 6073–6078 (2005).
13. Sylman, D., Micó, V., García, J. & Zalevsky, Z. Random angular coding for superresolved imaging. *Appl. Opt.* **49,** 4874–4882 (2010).
14. Park, Y. *et al.* Speckle-field digital holographic microscopy. *Opt. Express* **17,** 12285–12292 (2009).
15. Sheppard, C. Super-resolution in confocal imaging. *Optik* **80,** 53–54 (1988).
16. Müller, C. B. & Enderlein, J. Image scanning microscopy. *Phys. Rev. Lett.* **104,** 198101 (2010).
17. Ventalon, C. & Mertz, J. Quasi-confocal fluorescence sectioning with dynamic speckle illumination. *Opt. Lett.* **30,** 3350–3352 (2005).
18. Heintzmann, R., Jovin, T. M. & Cremer, C. Saturated patterned excitation microscopy—a concept for optical resolution improvement. *J. Opt. Soc. Am. A* **19,** 1599–1609 (2002).
19. Gustafsson, M. Nonlinear structured-illumination microscopy: wide-field fluorescence imaging with theoretically unlimited resolution. *Proc. Natl Acad. Sci. USA* **102,** 13081–13086 (2005).
20. Hell, S. W. & Wichmann, J. Breaking the diffraction resolution limit by stimulated emission: stimulated-emission-depletion fluorescence microscopy. *Opt. Lett.* **19,** 780–782 (1994).

Acknowledgements

The authors thank R. Heintzmann for a very nice suggestion concerning the blind-SIM algorithm. The authors also thank the anonymous referees for their constructive and stimulating remarks. This work was funded by the French Agence National de la Recherche (contract no. ANR-08-NANO-P053-36).

Author contributions

E.M., K.B., J.G. and A.S. conceived the blind-SIM approach and wrote the manuscript. E.M. and K.B. wrote the code and ran the model. J.G. performed the experiments and pre-processed the data. J.S. and C.N. prepared the samples. E.Le.M. and M.A. provided technical support and A.S. supervised the project.

Additional information

The authors declare no competing financial interests. Supplementary information accompanies this paper at www.nature.com/naturephotonics. Reprints and permission information is available online at http://www.nature.com/reprints. Correspondence and requests for materials should be addressed to A.S.